Conservative Finite Differences as an Alternative to Finite Volume for Compressible Flows

Jens Brouwer, Julius Reiss and Jörn Sesterhenn

Abstract Finite Volume schemes are the natural choice when simulating flows with shocks, since conservation is essential in the physics and as such in the simulation of this phenomenon. But finite difference schemes can be conservative as well. Conservation requires in such schemes a high internal consistency of the spatial and the temporal discretization. We present a skew-symmetric finite difference scheme, which is fully conservative due to its consistency, still easy to implement and numerically efficient. A variety of different flow configurations containing shocks and turbulence are presented.

1 Introduction

Finite volume (FV) schemes and conservative schemes are so strongly connected, that often these two terms are used synonymously. Indeed all FV schemes conserve the quantities of the underlying discretized flux-equations. The inverse statement however is not true: A set of discrete equation can be conservative, even if a form other than the flux form is the starting point of the scheme. This extra freedom can be beneficial to fulfill additional requirements. In the case presented here this requirement is a low dissipation of the scheme. This allows the direct numerical simulation (DNS) of turbulence and acoustics. Further, a high discretization order in space and time is important to keep the computational cost of simulations of large physical systems as low as possible.

J. Brouwer (✉) · J. Reiss · J. Sesterhenn
TU Berlin, ISTA, Mueller-Breslau Str. 8, 10623 Berlin, Germany
e-mail: jens.brouwer@tnt.tu-berlin.de

J. Reiss
e-mail: julius.reiss@tnt.tu-berlin.de

J. Sesterhenn
e-mail: joern.sesterhenn@tu-berlin.de

J. Fuhrmann et al. (eds.), *Finite Volumes for Complex Applications VII - Methods and Theoretical Aspects*, Springer Proceedings in Mathematics & Statistics 77,
DOI: 10.1007/978-3-319-05684-5_15,

We use a skew-symmetric finite difference scheme which meets the afore mentioned properties, which builds on similar concepts as [4, 12]. As computational variables for the equations of compressible flow the quantities $(\sqrt{\rho}, \sqrt{\rho}u_\alpha, p)$ are used. The conserved quantities of mass, $\sum \sqrt{\rho}^2$, momentum, $\sum \sqrt{\rho}(\sqrt{\rho}u_\alpha)$, and total energy, $\sum p/(\gamma-1) + (\sqrt{\rho}u_\alpha)^2/2$, are a consequence of the consistency of the discrete equations *and* a proper time stepping. They are not enforced by formulating the balance of these terms as in FV methods. Arbitrary order in space and time can be achieved. The scheme is computationally efficient in space as it builds on (non-upwind) finite-differences and point-wise multiplication. However, for full conservation an implicit time stepping scheme is needed. The resulting nonlinear system is solved by fix point iterations which is found to converge satisfactory well for time steps similar to those of an explicit scheme.

We present resolved calculations of a turbulent and transonic boundary layers, as well as a Richtmyer-Meshkov instability and one-dimensional shock problems.

2 Numerical Scheme

Here we provide a short overview of the skew-symmetric finite-difference scheme. A detailed derivation and discussion is out of scope of this paper but can be found in [10] for the spatial discretisation and [2] for the time stepping procedure.

Compressible flow is described by the Navier-Stokes equations which state the evolution of mass, momentum and energy:

$$\partial_t \rho + \partial_{x_\beta} \rho u_\beta = 0 \tag{1}$$

$$\partial_t \rho u_\alpha + \partial_{x_\beta}(\rho u_\beta u_\alpha) + \partial_{x_\alpha} p = \partial_{x_\beta} \tau_{\alpha\beta} \tag{2}$$

$$\partial_t \left(\rho \left[e + \frac{u_\alpha u_\alpha}{2}\right]\right) + \partial_{x_\beta} \left(\rho u_\beta \left[e + \frac{u_\alpha u_\alpha}{2} + \frac{p}{\rho}\right]\right) = \partial_{x_\alpha} u_\beta \tau_{\alpha\beta} + \partial_{x_\alpha} \phi_\alpha. \tag{3}$$

The ρ is the density, u_α is the $\alpha^{th} = 1, 2, 3$ velocity component. Pressure is p and $\tau_{\alpha\beta} = \mu(\partial_{x_\alpha} u_\beta + \partial_{x_\beta} u_\alpha) + (\mu_d - \mu 2/3)\delta_{\alpha\beta}\partial_{x_\gamma} u_\gamma$ is the Newtonian friction. The heat flux is given by $\phi_\alpha = \lambda \partial_{x_\alpha} T$ with the heat conductivity λ. Ideal gas with the internal energy $e = (p/\rho)/(\gamma-1)$ and adiabatic exponent γ is assumed in the following. Summing convention is assumed.

A pure rewriting of the momentum equations leads to the equations in skew-symmetric form

$$\partial_t \rho + \partial_{x_\beta} \rho u_\beta = 0 \tag{4}$$

$$\frac{1}{2}\left(\partial_t \rho \cdot + \rho \partial_t \cdot\right) u_\alpha + \frac{1}{2}\left(\partial_{x_\beta} u_\beta \rho \cdot + u_\beta \rho \partial_{x_\beta} \cdot\right) u_\alpha + \partial_{x_\alpha} p = \partial_{x_\beta} \tau_{\alpha\beta} \tag{5}$$

$$\begin{aligned} &\frac{1}{\gamma-1}\partial_t p + \frac{\gamma}{\gamma-1}\partial_{x_\beta}\left(u_\beta p\right) - u_\alpha \partial_{x_\alpha} p \\ &\quad = -u_\alpha \partial_{x_\beta} \tau_{\alpha\beta} \partial_{x_\beta} u_\alpha \tau_{\alpha\beta} + \partial_{x_\alpha} \phi_\alpha \end{aligned} \tag{6}$$

It is understood that the space and time derivatives in the first two terms of (5) act also on u right of the parentheses, which is marked by a „·". The momentum equation is called skew-symmetric, because the resulting spatial and temporal differentiation operators are skew-symmetric. The skew-symmetry of these operators leads to the analytical conservation of mass, momentum and energy. The kinetic energy was split from the total energy equation to arrive at an equation for the internal energy. To preserve the skew-symmetry in the discretization, skew symmetric derivative matrices $D^T = -D$ are used.

Morinishi's rewriting, [7], transforms the time derivative in the momentum equations (5) to $\frac{1}{2}\left(\partial_t \rho \cdot + \rho \partial_t \cdot\right) u_\alpha = \sqrt{\rho}\partial_t(\sqrt{\rho}u_\alpha)$. and leads to:

$$\sqrt{\rho}\partial_t(\sqrt{\rho}u_\alpha) + \frac{1}{2}\left(\partial_{x_\beta} u_\beta \rho \cdot + u_\beta \rho \partial_{x_\beta} \cdot\right) u_\alpha + \partial_{x_\alpha} p = \partial_{x_\beta}\tau_{\alpha\beta}. \tag{7}$$

The convective term $\frac{1}{2}\left(\partial_{x_\beta} u_\beta \rho \cdot + u_\beta \rho \partial_{x_\beta} \cdot\right)$ becomes a skew symmetric matrix $D^{\mathbf{u}}$, if discretized appropriately. By multiplying it by u_α^T

$$u_\alpha^T \sqrt{\rho}\partial_t(\sqrt{\rho}u_\alpha) + u_\alpha^T D^{\mathbf{u}} u_\alpha + u_\alpha^T \partial_{x_\alpha} p = u_\alpha^T \partial_{x_\beta}\tau_{\alpha\beta} \tag{8}$$

the change of kinetic energy is derived. Skew-symmetry implies $u_\alpha^T D^{\mathbf{u}} u_\alpha = 0$, thus

$$\frac{1}{2}\partial_t(\sqrt{\rho}u_\alpha)^2 = -u_\alpha^T \partial_{x_\alpha} p + u_\alpha^T \partial_{x_\beta}\tau_{\alpha\beta}.$$

The transport term conserves the kinetic energy; the kinetic energy is changed by pressure work and friction alone, as in the analytical theory, but in contrast to standard schemes. Now, also the unusual appearance of $\sqrt{\rho}$ instead of ρ in the momentum equation can be understood. It is the quadratic splitting of the kinetic energy. The terms $u_\alpha \partial_{x_\alpha} p - u_\alpha \partial_{x_\beta}\tau_{\alpha\beta}$ in Eq. (6) balance the change of kinetic energy by an according change of the internal energy, so that total energy is conserved. This structure carries over to the discrete case. Momentum conservation can be derived in a similar manner.

The method can be easily applied to transformed, structured grids, meaning grids generated by C^1 mappings of the unit cube. The conservation properties are strictly fulfilled as before. The resulting equations are

$$\begin{aligned}
&J 2\sqrt{\rho}\partial_t\sqrt{\rho} + \partial_{\xi^\beta}\tilde{u}_\beta \rho = 0\\
&J\sqrt{\rho}\partial_t(\sqrt{\rho}u_\alpha)u_\alpha + \frac{1}{2}\left(\partial_{\xi^\beta}\tilde{u}_\beta \rho \cdot + \tilde{u}_\beta \rho \partial_{\xi^\beta}\cdot\right) u_\alpha + J\partial_{x_\alpha} p = \partial_{\xi_\beta}\tilde{\tau}_{\alpha\beta}\\
&J\frac{1}{\gamma-1}\partial_t p + \frac{\gamma}{\gamma-1}\partial_{\xi^\beta}\left(\tilde{u}_\beta p\right) - J u_\alpha \partial_{x_\alpha} p\\
&\quad = -u_\beta \partial_{\xi^\alpha}\tilde{\tau}_{\alpha\beta} + \partial_{\xi^\alpha} u_\beta \tilde{\tau}_{\alpha\beta} + \partial_{\xi^\alpha}\tilde{\phi}_\alpha.
\end{aligned}$$

The effective velocities are defined to include the metric factors $\tilde{u}_{\gamma_1} = (\mathbf{e}_{\gamma_2} \times \mathbf{e}_{\gamma_3})\mathbf{u}$, γ_1 cyclic. The local basis vectors are defined as $\mathbf{e}_\alpha = \partial_{\xi^\alpha}\mathbf{r}$, with $r = (x, y, z)^T$. The Jacobian is $J = (\mathbf{e}_1 \times \mathbf{e}_2) \cdot \mathbf{e}_3$.

The discretization is done in a straight forward manner with the variables $(\sqrt{\rho}, \sqrt{\rho}u_\alpha, p)$. All derivatives are replaced by skew-symmetric derivative matrices (i.e. symmetric stencils). At boundaries the summation by parts property is assumed for which explicit derivatives constructed by Strand are used [11]. Details on the boundary treatment can be found in [10]. In addition, the use of SBP matrices allows the implementaion of an effevtive multiblock decomposition of the domain.

Time integration

The conserved quantities are (partly) quadratic forms of the discretization variables. Quadratic quantities are in general not conserved. Runge-Kutta schemes conserve quadratic invariants when the coefficients of their Butcher table fulfill the condition

$$b_i a_{ij} + b_j a_{ji} = b_i b_j. \tag{9}$$

This restrictive requirement is fulfilled by all Gauss-collocation methods, a family of s-stage implicit RK schemes of order $2s$. Time integration is done by the two stage, fourth order method:

$$\begin{array}{c|cc} \frac{1}{2} - \frac{\sqrt{3}}{6} & \frac{1}{4} & \frac{1}{4} - \frac{\sqrt{3}}{6} \\ \frac{1}{2} + \frac{\sqrt{3}}{6} & \frac{1}{4} + \frac{\sqrt{3}}{6} & \frac{1}{4} \\ \hline & \frac{1}{2} & \frac{1}{2} \end{array}$$

These methods lead to full conservation, which is discussed in [3]. It is found that a fix point iteration works surprisingly well for moderate Δt. It is further observed, that the conservation converges quicker than one might estimate form the convergence of the full solution.

3 Numerical Examples

In this section we present four numerical examples to show the applicability of our method to physical flow situations containing small scale turbulence and shocks. Therefore we show computations of a classical shock-tube test case, a turbulent boundary layer, a developing Richtmyer-Meshkov instability and an instationary shock-wave/boundary-layer interaction (*SBLI*). All simulations use the previously described skew-symmetric finite difference scheme. The implementation is in FORTRAN and parallelized using MPI directives. Spatial discretization is done using 6th order central differences with SBP properties. Temporal discretizations is achieved by the implicit 4th order Gauss collocation method with one small exception. Due to the higher computational effort of the implicit scheme, the SBLI simulation is advanced in time until initial transients are gone using an explicit Runge-Kutta scheme of

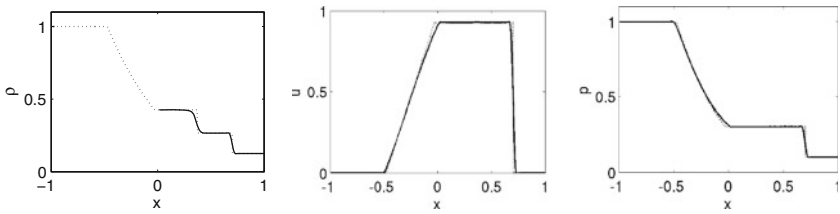

Fig. 1 Sod's test case at $t = 0.4$ using the Shock filter of Bogey et al. [1]. Good agreement is found. The Shock speed matches the analytical solution (*dotted line*)

fourth order. Once a statistically steady regime is reached, integration using the fully conservative Gauss-collocation scheme is resumed.

Sod's test case

The first test case is the classical Sod's shock-tube problem for the Euler equations. Starting conditions are $q^l = (1, 0, 1)$ and $q^l = (0.125, 0, 0.1)$ where $q = (\rho, u, p)$. The problem is discretized using 201 points and Bogeys conservative shockfilter is applied, see [1] for details. Figure 1 shows a comparison between the numerical and analytical solution, displaying agreement of propagation speed with the analytical solution, as expected for a conservative scheme. Only the contact discontinuity shows slightly higher damping than needed. The filter method is independent of the base scheme and can be easily modified to improve this.

DNS of a turbulent boundary layer at $Re \approx 5000$

To show the validity of the skew-symmetric finite-difference approach to small scale turbulence a direct numerical simulation of a turbulent boundary layer is shown. Reynolds number $Re_{\delta_{in}} = 4736$ and free-stream Mach number $M = 0.8$, where δ_{in} is the 99 % boundary layer thickness. The computational domain of dimensions $[106\delta_{in} \times 8\delta_{in} \times 9\delta_{in}]$ is resolved using roughly 80 million grid points. This resolution is chosen so that the grid spacing at the wall satisfies a dimensionless wall distance of $\Delta y^+ < 1$. Throughout the domain and the average Δy^+ at the boundary layer edge is not larger than 7. The turbulent inlet conditions are enforced using a recycling/rescaling method as introduced by Lund [6], and modified by Pirozzoli [9]. Results are in good agreement with reference computations of Pirozzoli et al. [8]. Figure 2 depicts streamwise velocity in a wall-parallel plane where the formation of characteristic streak structures is visible.

2-Dimensional Richtmyer-Meshkov instability

A Richtmyer-Meshkov instability is an instability mechanism that develops when an interface between fluids is impulsivly accelerated by a passing shockwave. In our simulation the fluid-fluid interface is modeled by a discontinous jump in density. The shock Mach number of the accelerating shockwave is $M_s = 1.5$. The two-dimensional domain is discretized with $[4096 \times 2048]$ gridpoints and the afore mentioned conservative shock-filter by Bogey et al. is used. Figure 3 shows the

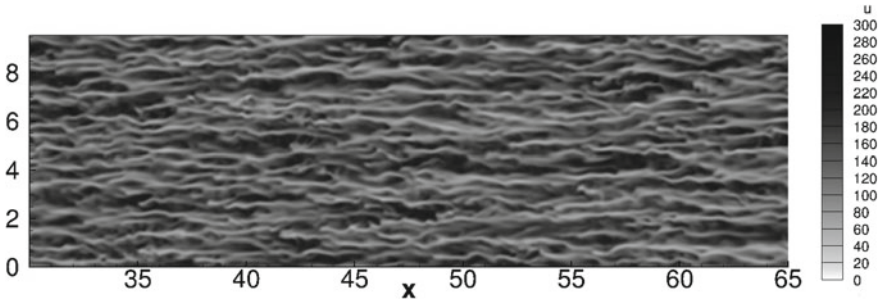

Fig. 2 Contours of instantaneous streamwise velocity in a xz-plane located at $y^+ \approx 10$

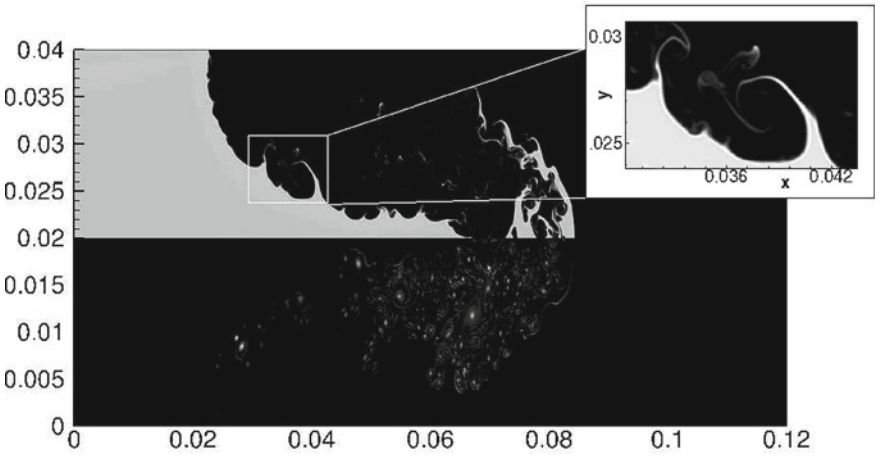

Fig. 3 Contour plot of a 2-dimensional Richtmyer-Meshkov instability; the *top* half of the domain depicts density while vorticity is shown in the *lower* half

mushroom-like growth out of the fluid interface. In the top half of the figure density contours are plotted while the lower half depicts vorticity. Due to the minimal dissipation of the skew-symmetric scheme, many secondary and even tertiary instabilities can be observed. The prime examples being the Kelvin-Helmholtz instabilities that form at the shear-layer between the two fluids. The vorticity plot reveals the complex turbulent flow field in the vicinity of the large scale structure that drives the creation of many of the smaller instabilities.

Shock-wave/boundary-layer Interaction

Shock-wave/boundary-layer interactions can occur in many important engineering applications. A prominent example is transonic flow over an airfoil, as the flow is accelerated over the airfoil, a super-sonic pocket forms that is terminated by a shock. The strong pressure gradient leads to the separation of the boundary-layer behind the shock and a recirculation bubble forms. Under certain conditions the shock can

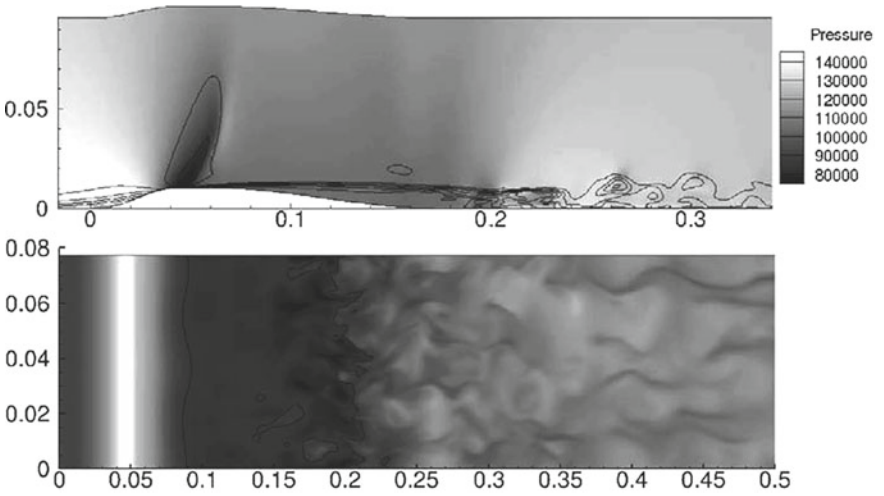

Fig. 4 *Top*: Snapshot of the transonic flow over a bump. Pressure contours and iso-lines of stream-wise velocity behind the bump are displayed. *Bottom*: Instantaneous streamwise velocity contours in wall-parallel plane at $y^+ \approx 25$. The current location of the recirculation bubble is marked by the $u = 0$ iso-line

exhibit large scale movements which has disastrous influence on all aerodynamic quantities. For a comprehensive review of the different forms of transsonic SBLI see e.g. [5].

The phenomenon of Shock-wave/boundary-layer interaction was one of the main motivations for the development of the conservative finite-difference scheme, as the simulation has to resolve the small turbulent scales in the boundary layer as well as to handle the shock movements. The simulations shown below are preliminary studies of SBLI occurring due to transonic flow over a bump. A laminar boundary layer is impinging on a small bump, a shock forms over the bump and a recirculation bubble that exhibits small breathing motions forms behind the interaction. Past the interaction zone the boundary layer begins its transition to turbulence. The size of the computational domain is $[65 \times 20 \times 12]$ measured in inlet boundary layer thicknesses δ_{in} and is resolved using approximately 20 million grid points. The maximum height of the bump is $1.2\delta_{in}$ while its length is $21.9\delta_{in}$. Shown below are snapshots of the instantaneous velocity and pressure fields. In Fig. 4 the geometry of the case is visible. The shock is visible both in the pressure fields and the contourlines of the stream-wise velocity. The recirculation bubble in the snapshot can be seen extending up to $x \approx 0.2$. In the lower panel of the figure the stream-wise velocity in a wall-parallel plane is shown. Again, the position of the shock at $x = 0.05$ and the length of the recirculation bubble can be seen. In addition the transition of the laminar flow field to turbulence through the interaction zone is visible.

4 Conclusions

We presented a fully conservative finite-difference scheme for the compressible Navier-Stokes equations on arbitrarily distorted, structured grids. In addition to its energy preserving nature the scheme introduces no artificial dissipation. The scheme is shown to be applicable to physical situations containing shocks and small scale turbulence while being easy to implement. This makes the skew-symmetric finite difference discretization a worthy alternative to Finite Volume methods in the context of large and small scale simulations of compressible flow.

References

1. Bogey, C., De Cacqueray, N., Bailly, C.: A shock-capturing methodology based on adaptative spatial filtering for high-order non-linear computations. JCP **228**(5), 1447–1465 (2009)
2. Brouwer, J., Reiss, J., Sesterhenn, J.: Fully conservative finite-difference schemes of arbitrary order for compressible flow. AIP Conf. Proc. **1479**(1), 2290–2293 (2012)
3. Brouwer, J., Reiss, J., Sesterhenn, J.: Conservative time integrators of arbitrary order for finite-difference discretization of compressible flow (2013). Submitted to Computers & Fluids
4. Kok, J.: A high-order low-dispersion symmetry-preserving finite-volume method for compressible flow on curvilinear grids. JCP **228**(18), 6811 (2009)
5. Lee, B.: Self-sustained shock oscillations on airfoils at transonic speeds. Prog. Aerosp. Sci. **37**(2), 147–196 (2001)
6. Lund, T.: Generation of turbulent inflow data for spatially-developing boundary layer simulations. JCP **140**, 233–258 (1998)
7. Morinishi, Y.: Forms of convecction and quadratic conservative finite difference schemes for low mach number compressible flow simulations. Trans. Jap. Soc. Mech. Eng. B (2007)
8. Pirozzoli, S., Bernardini, M.: Turbulence in supersonic boundary layers at moderate reynolds number. J. Fluid Mech. **688**, 120 (2011)
9. Pirozzoli, S., Bernardini, M., Grasso, F.: Direct numerical simulation of transonic shock/ boundary layer interaction under conditions of incipient separation. JFM **657**, 361 (2010)
10. Reiss, J., Sesterhenn, J.: A conservative, skew-symmetric finite difference scheme for the compressible navier-stokes equations. Accepted by Computers and Fluids
11. Strand, B.: Summation by parts for finite difference approximations for d/dx. JCP **110**, 47 (1994)
12. Verstappen, R., Veldman, A.: Symmetry-preserving discretization of turbulent flow. JCP **187**(1), 343 (2003)